https://dx.doi.org/10.1016/j.ijhydene.2022.05.067

Dynamic hierarchical modeling and control strategy of high temperature proton exchange electrolyzer cell system

Dongqi Zhao[a], Zhiping Xia[a], Meiting Guo[b], Qijiao He[b], Qidong Xu[b], Xi Li[a, c]*, Meng Ni[b]*

a. School of Artificial Intelligence and Automation, Key Laboratory of Image Processing and Intelligent Control of Education Ministry, Huazhong University of Science and Technology, Wuhan, Hubei, China.
b. Department of Building and Real Estate, Research Institute for Sustainable Urban Development (RISUD) and Research Institute for Smart Energy (RISE), The Hong Kong Polytechnic University, Hung Hom, Kowloon, Hong Kong.
c. Shenzhen Huazhong University of Science and Technology Research Institute, Shenzhen, Guangdong, China
*Corresponding author: Xi Li and Meng Ni.
E-mail address: lixi_wh@126.com (Xi Li), meng.ni@polyu.edu.hk (Meng Ni).

Abstract

High temperature proton exchange membrane electrolyzer cells (HT-PEMECs) show faster reaction kinetics than the low temperature PEMECs (LT-PEMECs) and are suitable for utilizing waste heat from the industry. However, dynamic modeling and control of HT-PEMECs are still lacking, which is critical for integrating the HT-PEMECs with fluctuating renewable power. In this study, hierarchical models are developed to investigate the transient behavior of the HT-PEMEC system with hydrogen recirculation. It is observed that the maximum efficiency point of the reference power can be reached by cooperatively adjusting the current density and anode inlet gas flow rate, and the application of artificial neural networks can accurately predict the operating conditions at the points of maximum efficiency. Moreover, the proposed cooperative model predictive control strategy not only improves the

efficiency (about 1.2%) during dynamic processes but also avoids the problem of reactant starvation. This study provides useful information to understand the dynamic behaviors of HT-PEMECs driven by excess renewable power.

Keywords: Hierarchical system model; Multiphysics analysis; Hydrogen recirculation system; System identification; Cooperative model predictive control.

Nomenclature

Abbreviation

HT-PEMEC	High temperature proton exchange membrane electrolyzer cell
MSE	Mean square error
CMPC	Cooperative model predictive control
MPC	Model predictive control
SOA	Seeker optimization algorithm
RMSE	Root mean square error
ANN	Artificial neural network
LHV	Low heating value

Roman

B_0	Permeability coefficient, m^2
C_p	Heat capacity at constant pressure, $J•mol^{-1}•K^{-1}$
E_{act}	Activation energy, $J•mol^{-1}$

D_i^{eff}	Effective diffusivity of species i, $m^2 \cdot s^{-1}$
D_{ik}^{eff}	Knudsen diffusion coefficient of i, $m^2 \cdot s^{-1}$
D_{im}^{eff}	Molecular diffusion coefficient of i, $m^2 \cdot s^{-1}$
i	Operating current density, $A \cdot m^{-2}$
V_{Nernst}	Equilibrium Nernst potential, V
F	Faraday constant, 96485 $C \cdot mol^{-1}$
$E_{H_2}^0$	Standard equilibrium potential for hydrogen oxidization, V
i_0	Exchange current density, $A \cdot m^{-2}$
N_i	Flux of mass transport, $kg \cdot m^{-3} \cdot s^{-1}$
y_i	Mole fraction of component i
n	Number of electrons transferred per electrochemical reaction
$P_{O_2}^L$	Local O_2 partial pressures, Pa
$P_{H_2}^L$	Local H_2 partial pressures, Pa
$P_{H_2O}^L$	Local H_2O partial pressures, Pa
R	Gas constant, 8.314 $J \cdot mol^{-1} \cdot K^{-1}$
u	Velocity field, $m^3 \cdot s^{-1}$
T	Temperature, K
S_{he}	Heat exchange area of heat exchanger, m^2
h_{he}	Convection coefficient of heat exchanger, kW m^{-2} K^{-1}

1. Introduction

The large-scale application of renewable energy is a promising way to tackle greenhouse gas emissions and energy shortages, while the intermittency and uncertainty of renewable energy pose a challenge to the stability of the grid [1-4]. Furthermore, hydrogen energy is regarded as an effective solution to mitigate energy fluctuations due to its cleanliness and high theoretical heating value. Collaborative operation of the fuel cell and electrolyzer cell enables efficient conversion between electricity and electrochemical energy [5, 6].

Currently, the proton exchange membrane electrolyzer cells (PEMECs) are very suitable for grid energy management due to their high current density, excellent dynamic performance, high efficiency and fast start/stop compared to alkaline electrolyzers, which are mainly attributed to the more compact structure and avoidance of electrolyte cycles [7-11]. In recent years, the development of membranes enables PEMECs to operate at higher temperatures (120℃-180℃), which increases the electrochemical reaction kinetics and decreases the electrical energy demand [12-14]. Compared with high temperature solid oxide electrolyzer cells (SOECs) working at about 800℃, HT-PEMECs do not require very high temperature thermal energy. Thus, HT-PEMEC can make use of a wider range of industrial waste heat electrolytic hydrogen production. Besides, to ensure the dynamic performance and long-life operation of HT-PEMEC, dynamic behavior analysis and control strategy design are necessary.

HT-PEMECs are widely studied due to the advantages mentioned above. Jin et al. [15] used a one-step method to synthesize 4-acetylpyridine and para-terphenyl/biphenyl into a high performance membrane, which was detected with high electrical conductivity of 0.102 S cm^{-1} at 180 ℃ and excellent stability. Hansen et al. [16] developed an Aquivion^{TM} membrane and tested it for electrolysis reaction at 130 ℃ and ambient pressure. It was found that the tantalum coating shows adequate corrosion resistance and electrical conductivity at high current densities, and hot pressing operations before cell assembly can enhance cell performance. Dong

et al. [17] found that introducing porous structures into high temperature proton exchange membranes effectively improves proton conductivity, however, excessive porosity may lead to degraded cell performance due to high permeability.

Besides experimental studies, cell-level and system-level simulation studies have also been extensively carried out. Garbe et al. [18] used a combination of numerical calculation and electrolysis experiments to propose that the conversion efficiency of high temperature operating (120 ℃, 50 μm membrane) is 14% higher than the usual operating (60 ℃, 180 μm membrane) at 3 A cm^{-2}. Gunay et al. [19] used machine learning and principal component analysis to predict the polarization curves of different electrode materials, and the root mean square error (RMSE) was only 0.18. Ruiz et al. [20] used the finite volume method to analyze the effect of three different flow channels (Parallel, serpentine and multiple serpentines) on hydrogen production, and found that multiple serpentines flow channel has a significant advantage for electrolysis performance and temperature gradient. Zhang et al. [21] used the finite element method to investigate the effects of the co-flow channel and counter-flow channel on the multiphysics field of the electrolyzer cell, showing that the counter-flow channel has lower temperatures and higher temperature gradients. Bonanno et al. [22] conducted an energy and exergy analysis of a high temperature proton exchange membrane electrolyzer cell and found that it exhibited higher exergy efficiency at the self-heating maintained state. Toghyani et al. [23] used numerical calculations to study the effects of temperature, cathode pressure, membrane thickness and gas diffusion layer thickness on the efficiency and exergoeconomic analysis of electrolyzer, which found that high temperature, high pressure and thin membrane significantly reduced the exergy cost. Nafchi et al. [24] analyzed the effect of operating conditions on system performance, combining the electrolyzer with photovoltaic and thermal storage systems, and observed that increased pressure and membrane thickness significantly reduce system efficiency.

In summary, current simulation work has focused on the effects of flow channel design and operating parameters on the HT-PEMEC, however transient performance, which is critical to the application of electrolyzer cells for energy management, has rarely been investigated. In this study, in order to achieve high accuracy and fast simulation, the hierarchical model is developed to explore the dynamic performance of the hydrogen recirculation system, which combines the multiphysics model to describe electrolyzer with lumped parameter models to describe sub-systems. Dynamic performance of the electrolyzer cell can be accurately described as well as avoiding the huge computational costs associated with system models described by the finite element method. On this basis, model-based control strategies are designed to achieve fast and efficient transient processes and avoid reactant starvation problems. This study can provide a reference for the system integration and control research of hydrogen recirculation structures.

2. Hydrogen recirculation system structure

Steam produced by the evaporator is preheated, passes through the heat exchanger and heater, and finally is fed into the anode. Moreover, the cathode uses part of the electrochemically generated hydrogen as a carrier gas, instead of using steam. Compared with steam as the carrier gas, hydrogen recirculation systems significantly reduce the thermal energy requirements although they slightly increase the electrical energy requirements due to the increased Nernst voltage, which improves the overall system efficiency [25]. The detailed HT-PEMEC system structure is shown in Fig. 1a.

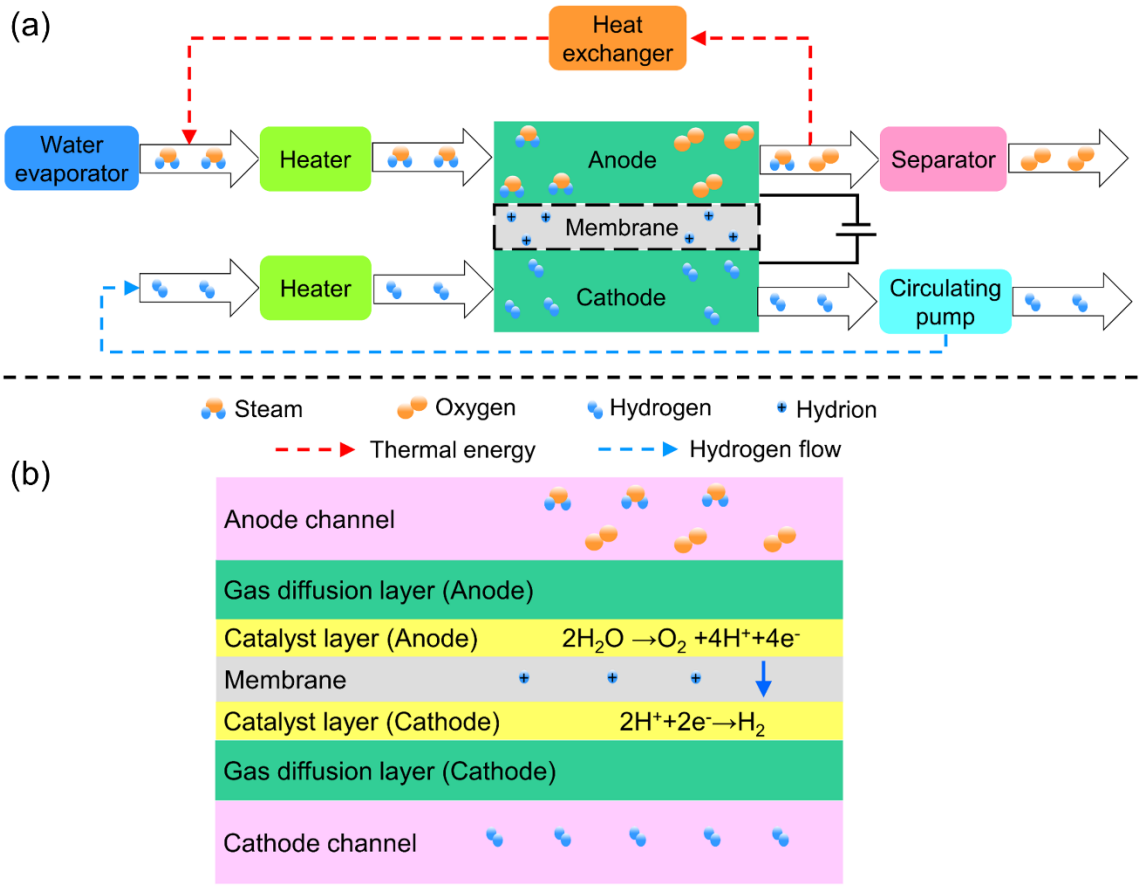

Fig. 1. (a) Hydrogen recirculation HT-PEMEC system structure; (b) Schematic diagram of HT-PEMEC.

3. Model development

3.1 Computational domain and assumptions

The multiphysics model based on the finite element method is widely used in the study of electrolyzer cells and fuel cells due to its accuracy, however, the method requires high computational resources and hence is not suitable for study at a system level, especially for studying the dynamic behavior of a system. Therefore, the hierarchical model of hydrogen recirculation system utilizes finite element methods to calculate electrochemical reactions, gas diffusion, proton/electron transport, and heat transfer of electrolyzer. Apart from that, other components use lumped parameter models to simplify the system calculation processes.

The computational domain of HT-PEMEC, which includes the gas channel, gas diffusion layer, catalyst layer and proton exchange membrane, is shown in Fig. 1b. Moreover, the

electrochemical reactions of the anode and cathode are respectively shown as follows.

$$\text{Anode: } 2H_2O \rightarrow O_2 + 4H^+ + 4e^- \quad (1)$$

$$\text{Cathode: } 2H^+ + 2e^- \rightarrow H_2 \quad (2)$$

The main assumptions are listed below: (1) Laminar flow is considered in the gas channel; (2) The membrane is impermeable to all gases; (3) The gas diffusion layer and the catalyst layer are isotropic porous media; (4) The catalyst is uniformly distributed in the catalyst layer [26, 27].

3.2 Governing equations

The applied voltage of the electrolyzer cell can be calculated as the sum of the Nernst potential (open circuit potential: OCP) and the overpotentials as [28, 29].

$$V_{cell} = E_{re}^0 + \frac{RT}{2F} ln \left[\frac{P_{H_2}^L (P_{O_2}^L)^{\frac{1}{2}}}{P_{H_2O}^L} \right] + \eta_{act} + \eta_{ohm} \quad (3)$$

Here $P_{H_2}^L$, $P_{O_2}^L$, and $P_{H_2O}^L$ denote the local partial pressures of the different gases rather than at the electrode surface, hence the concentration losses are included in Eq. (3). $E_{re}^0 + \frac{RT}{2F} ln \left[\frac{P_{H_2}^L (P_{O_2}^L)^{\frac{1}{2}}}{P_{H_2O}^L} \right]$ represents OCP. E_{re}^0 is the reversible potential of the electrolysis reaction under standard gas partial pressures, which represents the minimum potential demand and can be further expressed as Eq. (4) [30].

$$E_{re}^0 = 1.229 - 0.9 \times 10^{-3}(T - 298) \quad (4)$$

Activated overpotentials (η_{act}) are mainly associated with the microstructure and material of the electrode, which reflects the energy barrier of the electrochemical reaction, and can be calculated using the Buttler-Volmer equation [31].

$$i = i_0 \left\{ exp\left(\frac{\alpha n F \eta_{act}}{RT}\right) - exp\left(\frac{(1-\alpha) n F \eta_{act}}{RT}\right) \right\} \quad (5)$$

$$i_0 = \gamma \exp(-\frac{E_{act}}{RT}) \quad (6)$$

Here E_{act} represents the activation energy of the electrolysis reaction, α is the charge

transfer coefficient. n is the number of transferred electrons.

Ohmic overpotential reflects the resistance of the transfer of protons and electrons, and can be calculated by Ohm's law. The diffusion of gases in the gas channel and the porous electrode can be described by the extended Fick model [32].

$$N_i = -\frac{1}{RT}\left(\frac{B_0 y_i P}{\mu}\nabla P - D_i^{eff}\nabla(y_i P)\right) \text{ (i=1,2,…..n)} \quad (7)$$

$$D_i^{eff} = \frac{\varepsilon}{\tau}\left(\frac{1}{D_{im}^{eff}} + \frac{1}{D_{ik}^{eff}}\right)^{-1} \quad (8)$$

Here D_i^{eff} is the total effective diffusion coefficient. D_{im}^{eff} and D_{ik}^{eff} are related to molecular diffusion and Knudsen diffusion, respectively. The mass conservation of gases can be expressed as Eq. (9-10).

$$\nabla\left(-D_i^{eff}\nabla C_i\right) = R_i \quad (9)$$

$$\mathrm{R_{H_2O}} = -\mathrm{R_{H_2}} = -2\mathrm{R_{O_2}} = \frac{\mathrm{i}}{2\mathrm{F}} \quad (10)$$

Here R_i and C_i denote the mass source term and molar concentration of the gases, respectively. i is current density (A m^{-2}).

Flow field of gaseous components can be calculated using the Navier-Stokes equation with the Darcy term [33].

$$\rho\frac{\partial \mathrm{u}}{\partial \mathrm{t}} + \rho\mathrm{u}\nabla\mathrm{u} = -\nabla\mathrm{p} + \nabla\left[\mu(\nabla\mathrm{u} + (\nabla\mathrm{u})^T) - \frac{2}{3}\mu\nabla\mathrm{u}\right] - \frac{\varepsilon\mu\mathrm{u}}{B_0} \quad (11)$$

Temperature distribution of the electrolyzer cell can be described by the heat balance equation [34].

$$\rho\mathrm{C_p u}\bullet\nabla\mathrm{T} + \nabla(-\lambda_{\mathrm{eff}}\nabla\mathrm{T}) = \mathrm{Q} \quad (12)$$

$$\lambda_{\mathrm{eff}} = (1-\varepsilon)\lambda_{\mathrm{s}} + \varepsilon\lambda_{\mathrm{g}} \quad (13)$$

Here λ_{eff} represents the effective thermal conductivity, λ_{s} and λ_{g} correspond to the solid thermal conductivity and the gas thermal conductivity. Q represents the heat source term, which includes the generated thermal energy (Q_{Gen}) and consumed thermal energy (Q_{Con}) due

to the overpotential and electrolysis reactions, respectively.

$$\begin{cases} \mathrm{Q_{Gen}} = \mathrm{E_{Irr}} \times \mathrm{i} \\ \mathrm{Q_{Con}} = \mathrm{T\Delta S} \times \frac{\mathrm{i}}{\mathrm{2F}} \end{cases} \tag{14}$$

Here E_{Irr} represents the overpotential, including activation overpotential and ohmic overpotential. The overall overpotential measures the difference between the working voltage and the Nernst potential.

The steam supply subsystem can be described as a first-order system with a delay as follows [37].

$$\mathrm{G(s)} = \frac{1}{t_{con}s+1} e^{-t_d s} \tag{15}$$

Here t_{con} is the time constant, t_d is delay coefficient.

The lumped model of the heat exchanger can be expressed as Eqs. (16-18) [38].

$$\mathrm{NC_{ga}} \frac{\mathrm{dT_{ga.i}}}{\mathrm{dt}} = \dot{\mathrm{N}}_{\mathrm{in}} \mathrm{h_{in}} - \dot{\mathrm{N}}_{\mathrm{out}} \mathrm{h_{out}} + \sum \dot{\mathrm{Q}}_{\mathrm{tr}}, \mathrm{i} = \mathrm{off, in} \tag{16}$$

$$\rho_{\mathrm{s}} \mathrm{V_s C_s} \frac{\mathrm{dT_{he}}}{\mathrm{dt}} = \sum \dot{\mathrm{Q}}_{\mathrm{tr}} \tag{17}$$

$$\dot{\mathrm{Q}}_{\mathrm{tr}} = \mathrm{S_{he} h_{he}} (\mathrm{T_{ga.i}} - \mathrm{T_{he}}) \tag{18}$$

Here $\mathrm{T_{ga.i}}$ is the temperature of the high temperature off-gas and the low temperature inlet gas, $\mathrm{T_{he}}$ is the heat exchanger temperature.

Evaporator and heater can be considered as inputs of thermal energy [39].

$$\mathrm{Q_{heat}} = \dot{\mathrm{N}}_{\mathrm{gas}} (\mathrm{h_T} - \mathrm{h_{T_0}}) \tag{19}$$

Here h_T and h_{T_0} indicate the enthalpy of the gases respectively at the operating and ambient temperatures.

The energy efficiency of HT-PEMEC system can be expressed as the ratio of generated electrochemical energy to the sum of the input electrical and thermal energy [40].

$$\eta_{\mathrm{en}} = \frac{\mathrm{LHV_{H_2}} \times \dot{\mathrm{N}}_{\mathrm{H_2}}}{\mathrm{Q_{electric}} + \mathrm{Q_{thermal}}} \tag{20}$$

The HT-PEMEC model is solved using the finite element method, detailed information

about model validation and mesh independence can be found in the Refs [35, 36]. The anode and cathode outer boundaries were set as operating current density and zero potential, respectively. Inlet gas flow rates and temperatures were set at the anode and cathode inlets, and pressure conditions were set at the outlet. The top and bottom of the cell are set to be insulation. At each time step, the operating conditions (current density, inlet gas flow rate and inlet gas temperature) are solved by MATLAB and entered into COMSOL. Subsequently, the electrochemical model, mass transport, and heat transfer are solved by the MUMPS solver of the COMSOL, which utilizes the fully coupled method with constant newton nonlinearity.

Table 1. Geometric and physical parameters are applied in the model.

Parameter	value	unit
Channel height	1	mm
Channel width	1	mm
Channel length	50	mm
Gas diffusion layer thickness	0.38	mm
Membrane thickness	0.1	mm
Catalyst layer thickness	0.05	mm
Operating pressure	1	bar
Operating temperature	403.15	K
GDL permeability	1.18×10^{-11} [50]	m^2
Catalyst layer permeability	2.36×10^{-12} [50]	m^2
GDL porosity	0.4 [21]	
Porosity of catalyst layer	0.3 [21]	
Proton conductivity of electrolyte	20 [51]	S m^{-1}
Anode exchange current density	10^{-4} [29]	A cm^{-2}

Cathode exchange current density	0.1 [29]	A cm^{-2}
Number of cells	30	
Heat exchanger heat capacity	0.62 [37]	kJ kg^{-1} K^{-1}
Convection coefficient of heat exchanger	0.1	kW m^{-2} K^{-1}
Hydrogen recirculation ratio	0.2	
MPC predicted time domain length	10 [52]	
MPC control time domain length	3 [52]	
MPC control weighting factor	0.05 [52]	
Violation constraint penalty weight	1	
Steam utilization of SOA-PID	0.8	
SOA weight factor w_1	0.999 [53]	
SOA weight factor w_2	0.001 [53]	

4. Cooperative control strategy

The anode steam flow rate and current density are used as control parameters in the hydrogen recirculation system, and Fig. 2 shows the control structure of the hydrogen recirculation system. Neural network is trained to quickly and accurately predict the anode inlet steam flow rate by using the optimal operating conditions at different power consumptions. Subsequently, the predicted anode inlet gas flow rate is used as a feedforward control to regulate the steam supply subsystem, thereby avoiding the effects of system fluctuations on the steam supply subsystem. On the other hand, the hierarchical model is developed by combining the multiphysics model and lumped parameter model, while multiphysics models are not suitable for control strategy design. Therefore, the relationship between the current density and the power density consumed is obtained by the system identification method. Moreover, the

multiphysics model is utilized to analyze the effect of the change rate of current density on the dynamic behavior of the steam molar fraction in the anode catalyst layer, which avoids the problem of reactant starvation during dynamic processes. Finally, the identified model and constraint (maximum current density change rate) are imported into the model prediction controller to predict the dynamic behavior of the power density consumption and to control the HT-PEMEC system to track the reference power density consumption.

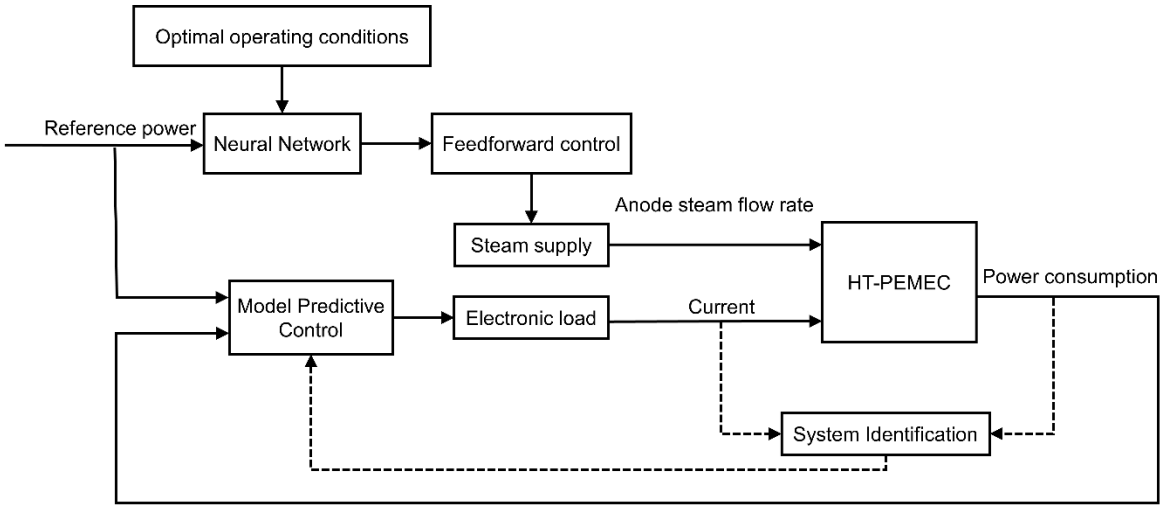

Fig .2. Cooperative control strategy structure for hydrogen recirculation system

4.1 Neural network predicts maximum efficiency point

In practice, the current and anode inlet gas flow rate are typically adjusted to control the working state of the electrolyzer system. It has been found by steady-state parameter analysis that the current density and anode inlet flow rate corresponding to each reference power can be cooperatively controlled to make the electrolyzer system work at the maximum efficiency points. Compared to voltage control schemes, current control schemes can directly reflect the extent of electrochemical reactions and thus avoid excessive overshoot, making the dynamic process easier to regulate [35]. As shown in Fig. 3c, the efficiency showed a trend of increasing first and then decreasing, and the current density corresponding to the maximum efficiency

point increases with the increase of the anode inlet flow rate. Further, most of the reactants are not utilized resulting in low efficiency at low current densities, thus efficiency increases with increasing current density. However, at high current densities, the overpotential loss is also high, resulting in low efficiency [41]. Moreover, dynamic switching between maximum efficiency points is essential for efficient operation [37-38]. Therefore, it is crucial that the maximum efficiency point corresponding to the reference power density is quickly and accurately predicted to provide information for the control strategy during the dynamic process. Artificial neural networks (ANN) are applied to predict the anode inlet gas flow rate corresponding to the maximum efficiency of reference power consumption due to its high accuracy and low computational cost.

The levenberg-marquardt method was applied to train the ANN, and the regressed R values for training and validation of the anode inlet flow rate are shown in Fig. 3a and Fig. 3b. Moreover, the mean squared errors of training and validation are $2.25e^{-9}$ and $2.34e^{-8}$, respectively. It is observed that the ANN can accurately predict the anode inlet flow rate corresponding to the maximum efficiency point.

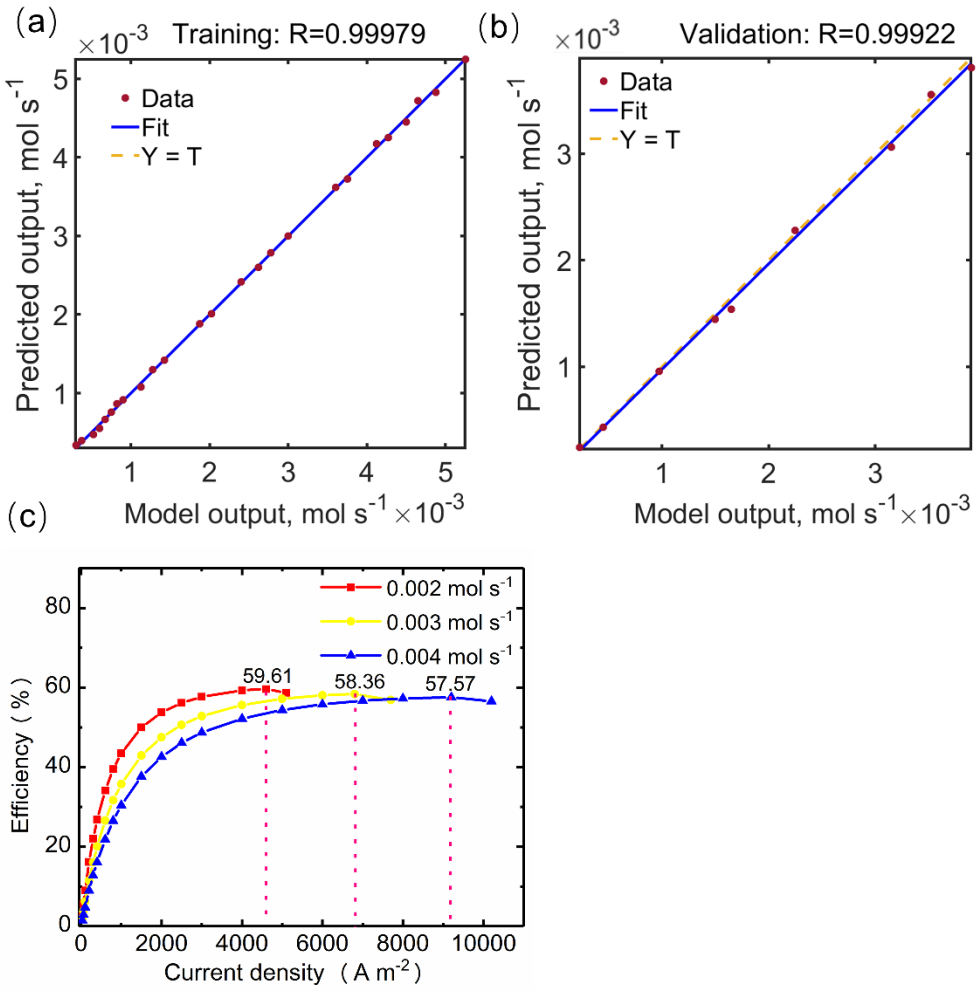

Fig. 3. (a) Training of artificial neural network to predict the anode gas inlet flow rate corresponding to the maximum efficiency point; (b) Validation of artificial neural network to predict the anode gas inlet flow rate corresponding to the maximum efficiency point; (c) Effect of anode gas flow rate on maximum efficiency point.

4.2 Limitation on the change rate of current density

During the dynamic process, fast electrochemical reactions and relatively slow gas transport may cause reactant starvation problems. Current density can directly reflect the degree of electrochemical reactions, therefore, the change rate of current density should be limited to prevent reactant starvation caused by severe electrochemical reaction fluctuations.

The initial operating point (500 A m^{-2}, 0.0009 mol s^{-1}) and the final steady-state operating

point (6500 A m^{-2}, 0.0045 mol s^{-1}) are set to investigate the transient behavior of reactant concentrations in the catalyst layer. To study the effect of different current density change rates on the reactant concentration in the catalyst layer during the transient process, the current density is set to different slope adjustment schemes while the anode inlet gas flow rate was adjusted by the same step adjustment scheme. Fig. 4a shows different current density change rates during the transient process, and Fig. 4b shows the transient behavior of steam molar fraction in the anode catalyst layer. It can be observed that when the current density changes drastically, the transient response of the steam molar fraction appears undershoot, which may cause the problem of reactant starvation during the transient process. Undershoot is triggered due to the drastic electrochemical reaction consuming a large amount of steam, while steam diffuses relatively slowly in the electrode, which may cause the catalyst to be oxidized at low steam concentration conditions. Therefore, the current density change rate should be limited to avoid the undershoot, and the maximum current density change rate was set to 2000 A m^{-2} s^{-1} in this dynamic study.

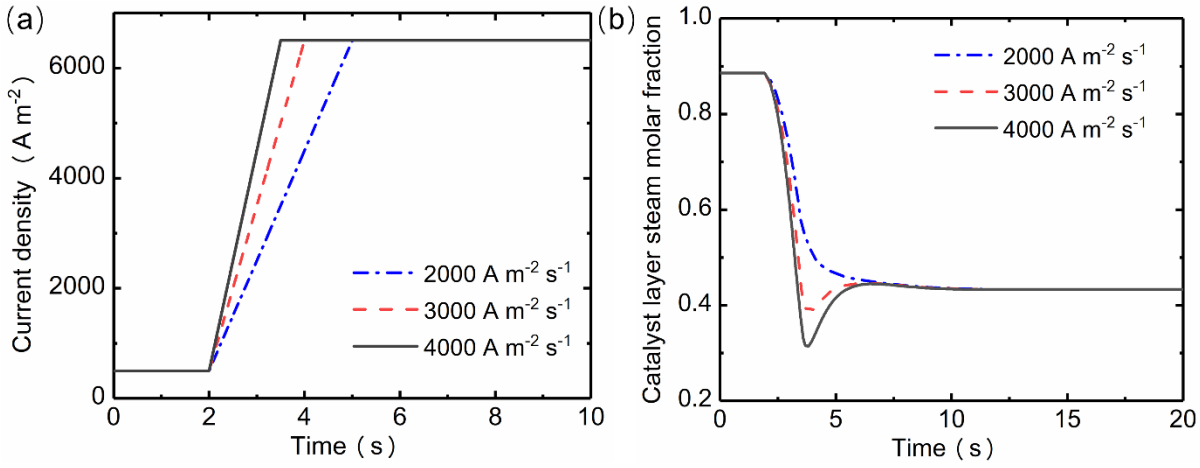

Fig. 4. (a) Current density changes during the dynamic process. (b) Transient response of the steam molar fraction in the anode catalyst layer.

4.3 System model identification

Multiphysics models are generally suitable for analyzing the multiphysics distribution and dynamic response of HT-PEMEC [42, 43], however, they are not suitable for the design of control strategies due to the inconvenience of obtaining state equations and transfer functions. Moreover, transfer functions and state equations are crucial for the design of complex control strategies, thus the system identification approach is employed to obtain the transfer functions of HT-PEMEC [44].

The input and output of the system identification are set as current density (A m^{-2}) and consumption power density (W m^{-2}), respectively, to obtain the relationship between them. Transient behavior between stochastic aperiodic steady-state operating conditions is acquired to enable the measured data to sufficiently reflect the dynamics of the HT-PEMEC system [45]. Moreover, the time interval allows the transient behavior to reach a steady state to obtain time-dependent parameters. To verify the accuracy of the identified model, two groups of data were obtained from the HT-PEMEC system, one group was utilized to identify the transfer function model, and the other group was used to verify the accuracy of the identified model. The two sets of data were sampled with an interval of 0.001 s and a duration of 700 s, and the identification data and verification data are presented in Fig. 5a and Fig. 5b.

The structure of the transfer function can usually be expressed as Eqs. (21-22).

$$\mathrm{Y(s)} = \frac{M(s)}{N(s)}U(s) + E(s) \tag{21}$$

$$\begin{cases} M(s) = b_0 s^m + b_1 s^{m-1} + b_2 s^{m-2} + \cdots + b_{m-1}s + b_m \\ N(s) = a_0 s^n + a_1 s^{n-1} + a_2 s^{n-2} + \cdots + a_{n-1}s + a_n \end{cases} \tag{22}$$

Where U(s), Y(s) and E(s) denote the Laplace transform of the input, output and noise, respectively. N(s) and M(s) represent the denominator and numerator polynomials, which define the relationship between the output and the input. Fit and mean squared error (MSE) are used to assess the accuracy of the identified model and they can be expressed as Eqs. (23-24).

$$\text{Fit} = \left(1 - \frac{\|y - \hat{y}\|}{\|y - \bar{y}\|}\right) \tag{23}$$

$$\text{MSE} = \frac{1}{N}\sum_{j=1}^{N}(y - \hat{y})^2 \tag{24}$$

Where y represents the multiphysics system model output, $\hat{y}$ denotes the identified model output, and $\bar{y}$ represents the average of y. N represents the amount of total data and j denotes the jth data. The relationship between the power consumption and current density is identified using System Identification Toolbox™ of Matlab, and the identified model can be described as Eq. 25.

$$\text{Y(s)} = \frac{1789s^3 + 1205000s^2 + 1630000s - 1726}{s^4 + 2987s^3 + 650700s^2 + 880900s + 0.5681}\text{U(s)} \tag{25}$$

The identified model outputs are compared with the HT-PEMEC system model for validation, which are shown in Fig. 5c and Fig. 5d using the identification data and validation data, respectively. Moreover, the results of Fit and MSE are presented in Table 2 and it can be found that the transfer function can adequately represent the dynamic behavior between the power consumption and the current density.

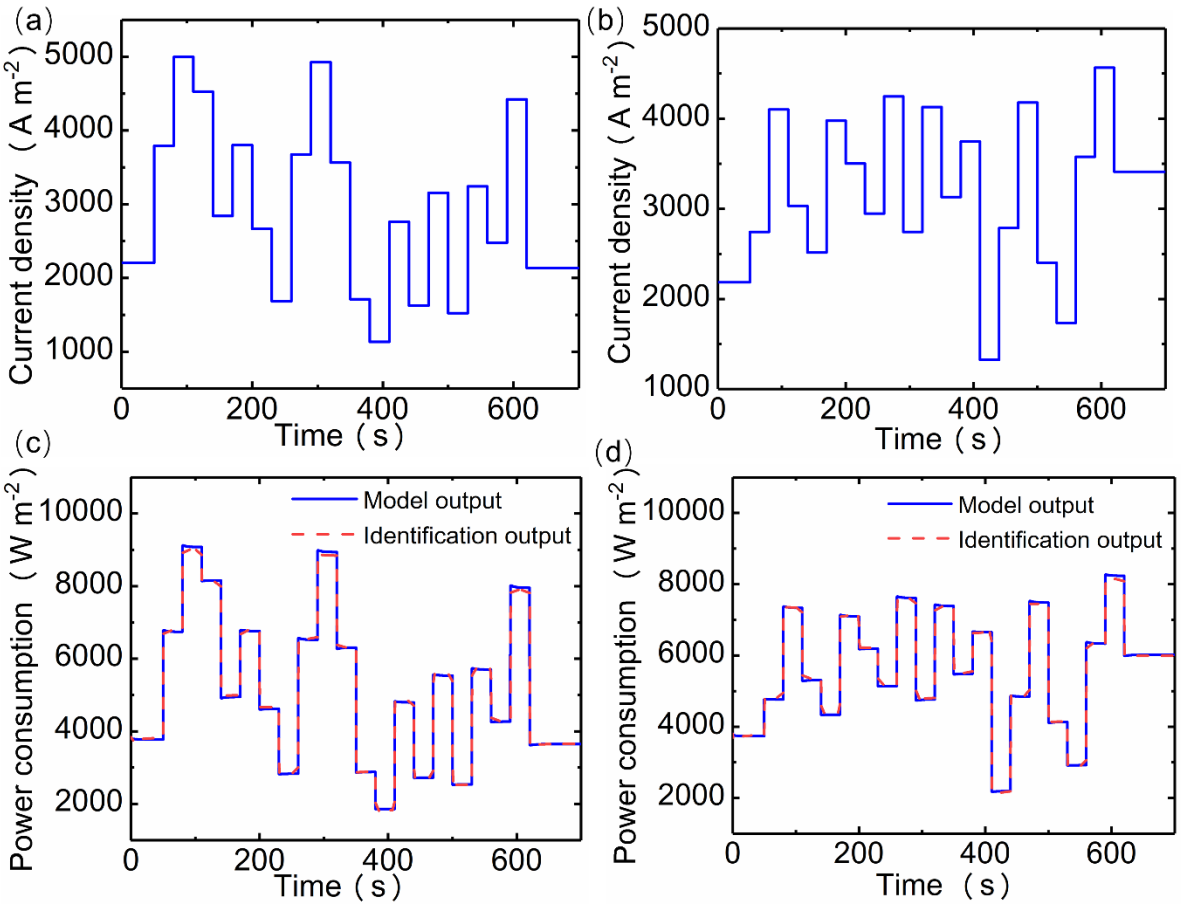

Fig. 5. (a) The varying current density data are used to identify the system model. (b) The varying current density data are used to validate the identified model. (c) Comparison of the identified model output with the identified data. (d) Comparison of the identified model output with the validation data.

Table 2. Identification model evaluation index.

Indicator	Identification data	Validation data
Fit	92.89 %	91.63%
MSE	21.74	26.99

4.4 Model predictive control

Model predictive control (MPC) strategy is an optimization control method that has been

widely used in the control design of dynamic systems [46, 47]. The workflow of the model predictive control strategy is shown in Fig. 6. At each time step, the MPC controller predicts the dynamic behavior of the HT-PEMEC system based on the identified system model and solves the optimization problem (Eq.22) according to the given maximum change rate of current density. The sequence of current density control actions is calculated by solving the optimization problem. However, only the first current density control action is applied to the MPC controller and subsequent control actions are ignored, in which the above cyclic process is repeated at each time step. Therefore, the model predictive control strategy enhances the dynamic performance of the HT-PEMEC system through real-time prediction and optimization.

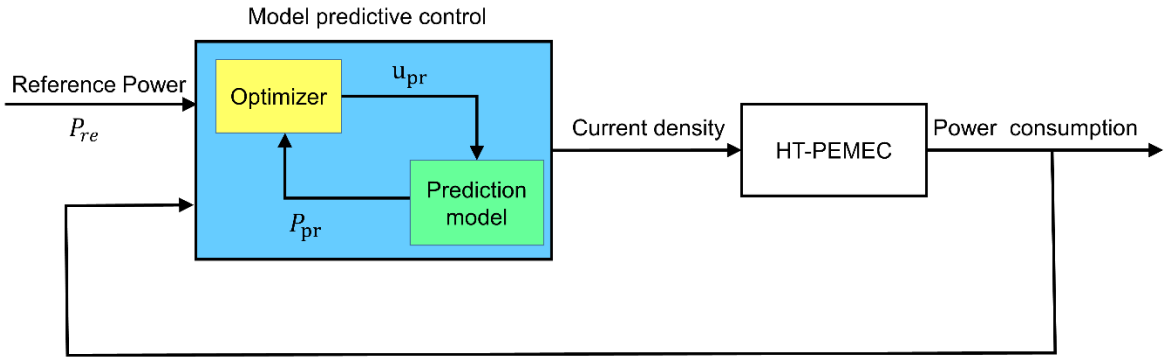

Fig. 6. Model predictive control strategy framework.

The optimization problem is solved by calculating the minimum value of the optimization equation, which is expressed as Eq. 26. Moreover, the optimization equation includes three parts: reference power tracking (J_{tra}), current density variation suppression (J_{sup}), and constraint violation penalty (J_{con}).

$$\begin{cases} J = J_{tra} + J_{sup} + J_{con} \\ J_{tra} = \sum_{i=1}^{N_p} \{P_{re}(k+j) - P_{pr}(k+j)\}^2 \\ J_{sup} = \rho \sum_{j=1}^{N_c} \{u_{pr}(k+j-1) - u_{pr}(k+j-2)\}^2 \\ J_{con} = \lambda \varepsilon_k^2 \end{cases} \tag{26}$$

Where N_p is the predicted time domain length, P_{re} is the reference power, P_{pr} is the predicted power consumption, N_c is the control time domain length, ρ represent the

weighting factor, u_{pr} denote the optimized current density input, λ is the violation constraint penalty weight, ε_k is the slack factor.

4.5 Reference control strategy

For comparison with the proposed cooperative model predictive control strategy, the PID control strategy with constant steam utilization was optimized and adopted in the hydrogen recirculation system. However, the parameter optimization of the PID controller is critical for enhancing the dynamic performance of the PEMEC system, therefore the seeker optimization algorithm (SOA) is used to determine the control parameters of the PID controller [48]. The structure of the SOA-PID control strategy is illustrated in Fig. 7, which shows that the control parameters of the PID controller are determined by the seeker optimization algorithm, whereas the anode steam flow rate is obtained by the fixed steam utilization.

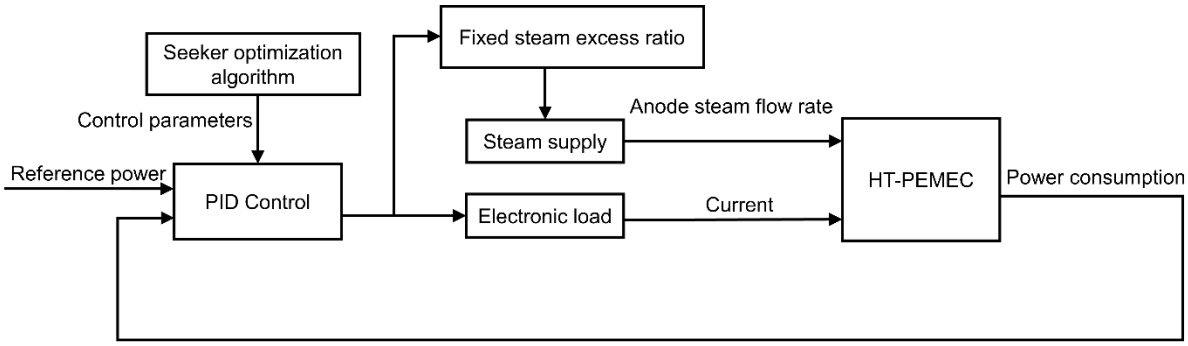

Fig. 7. SOA-PID control strategy framework

The control parameter optimization process of the seeker optimization algorithm is shown as follows.

(1) Initialize the position of each seeker, i.e., randomly generate the location information matrix;

(2) The adaptability of each seeker is calculated according to Eq. 27.

In order to obtain satisfactory dynamic performance, the time integral of the absolute value of the error is used as the objective function to find the minimum value. Moreover, the squared term of the control output is introduced to prevent excessive control actions.

$$F = \sum_1^j (w_1|e(t)| + w_2 u^2(t)) \quad (27)$$

Where $e(t)$ is the error, u(t) is control output, w_1 and w_2 represent weighting factor.

(3) The current position of each seeker is compared with the historical best position, and if the current position has a smaller objective function, the current position is taken as the historical best position. Subsequently, the next position is found by calculating the direction and step size, the detailed calculation process is described in Ref [49].

(4) If the end condition is not satisfied (maximum number of iterations and the specified minimum value of objective function), return to step 2.

5. Results and analysis

HT-PEMEC is a promising candidate for renewable energy storage, and excellent dynamic performance is critical for real-time energy management. However, fastly electrochemical reactions and slow gas diffusion processes may cause reactant starvation problems during dynamic processes. Therefore, safe, fast and efficient dynamic control strategies are essential for energy management and the long-life operation of the electrolyzer cell system. The cooperative model predictive control (CMPC) strategy is compared with SOA-PID to study dynamic response and reactant starvation problems.

5.1 Increased step response

To investigate the dynamic performance, cooperative model predictive control strategy and SOA-PID control strategy are used for a step response of 9000 W m^{-2} to 11000 W m^{-2}, and the sampling interval is set to 0.001s. The dynamic process of the power consumption is shown in Fig. 8a, and the cooperative model predictive control and SOA-PID control strategies reach steady state almost simultaneously. Compared to the SOA-PID control strategy, the power consumption change rate of the cooperative model predictive control strategy is relatively slow due to the limitation of the maximum current density change rate at the initial stage, and then

reaches steady state after a small overshoot. The cooperative model predictive control is an online optimization control strategy that predicts the dynamic behavior of the electrolyzer system to minimize the objective function (J) within the constraint of the maximum current density change rate, while the dynamic performance depends on the accuracy of the model estimation. However, the SOA-PID control strategy optimizes the output of the current density only based on the error between the reference power consumption and the actual power consumption. Therefore, as shown in Fig 8b, the current density change rate of the cooperative model predictive control is relatively small to suppress the sudden decrease of reactants during the dynamic process, after which a small overshoot is generated mainly due to the error between the model identification and the actual model.

The mass transfer process is slow compared to the electrochemical reaction, and drastic electrochemical changes may cause oxidation of the catalyst and degradation of the system performance during the dynamic process. Cooperative model predictive control not only uses the constraint of maximum current density change rate to suppress the reactant starvation problem, but also uses the neural network to calculate the inlet gas flow rate corresponding to the maximum efficiency point of power consumption in real-time and avoid the impact of power fluctuation on the inlet gas flow rate by feed-forward control. As shown in Fig. 8c, the cooperative model predictive control strategy can suppress the downward trend of the steam molar fraction at the catalytic layer during the dynamic process. However, the catalyst layer steam molar fraction of the SOA-PID control strategy shows an obvious downward trend, and the downward trend is more pronounced in the step from 9000 W m^{-2} to 12000 W m^{-2}. SOA-PID control strategy adjusts the current density according to the error between the reference power consumption and the actual power consumption leading to drastic changes in the current density at the initial stage, and the feedback control causes the reactants not to be supplied in time exacerbating the tendency of the reactant molar fraction downward. Therefore, compared

to the SOA-PID control strategy, the cooperative model strategy control can suppress the reactant starvation problem during the dynamic process.

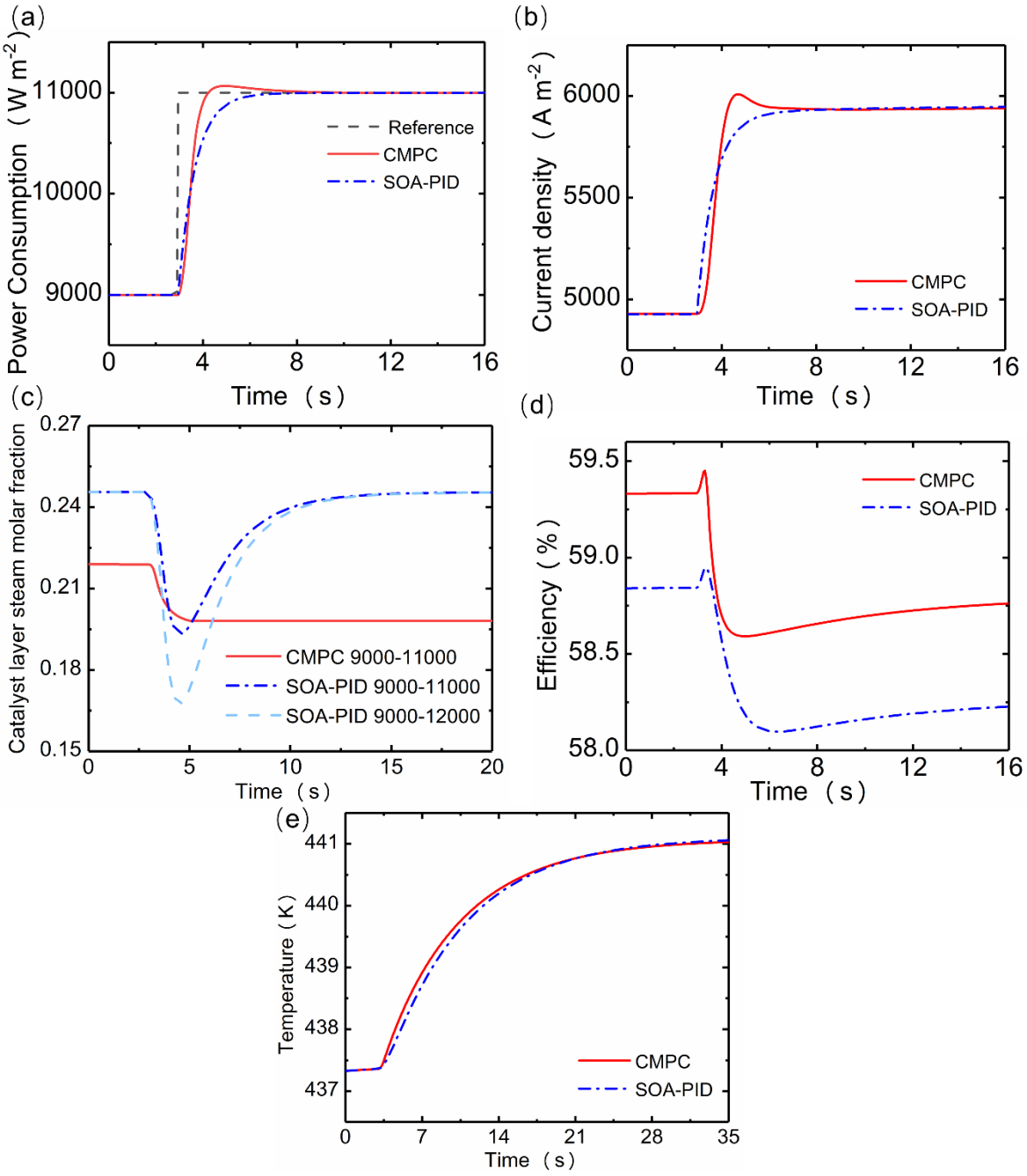

Fig. 8. (a) Power consumption transient response ; (b) Current density transient response; (c) Steam molar fraction transient response; (d) Energy efficiency transient response;(e) Operating temperature transient response.

In contrast to the constant steam utilization in the SOA-PID control strategy, artificial neural networks are used to calculate the inlet gas flow rate corresponding to maximum

efficiency of the reference power consumption in the cooperative model predictive control strategy, which makes the electrolyzer system reach the optimal operating condition and higher energy efficiency in the transient process. As shown in Fig. 8d, during the transient response, the rapid electrochemical reaction causes a slight increase in efficiency, however, the time lag of the elevated thermal energy demand due to the steam supply subsystem leads to a subsequent drop and finally a slow rise owing to the increased temperature (Fig. 8e).

5.2 Decreased step response

Cooperative model predictive control strategy and SOA-PID control strategy are compared during the transient step response 9000 W m^{-2} to 7000 W m^{-2}. As shown in Fig. 9a and Fig. 9b, the cooperative model predictive control strategy is still constrained by the maximum change rate of current density during the dynamic process of the decreased step, hence the power consumption response is slow in the initial phase and then reaches steady state after a negligible overshoot. Furthermore, smaller and smoother power consumption overshoot is observed during the reduced step process, meaning that model identification provides a more accurate estimate of the reduced step dynamic behavior. As shown in Fig. 9c, compared to the cooperative model predictive control strategy, the catalyst layer steam molar fraction shows a significant upward trend as well as being more pronounced during the larger decreased step (from 9000 W m^{-2} to 6000 W m^{-2}) at the SOA-PID control strategy, which implies a sudden decrease in fuel utilization and efficiency. Cooperative model predictive control utilizes an artificial neural network to calculate the inlet gas flow rate corresponding to the maximum efficiency of reference power consumption, thus making it more efficient during the dynamic process of the decreased step. In a typical response from 9000 W m^{-2} to 7000 W m^{-2}, the cooperative model predictive control strategy is approximately 1.2% more efficient compared to the SOA-PID control strategy and is shown in Fig. 9d. During the dynamic process, the fastly decreasing electrochemical reaction causes a slight decrease in efficiency, however, the time

lag of the reduced thermal energy demand due to the steam supply subsystem leads to a subsequent rise and finally a slow drop owing to the decreased temperature (Fig. 9e).

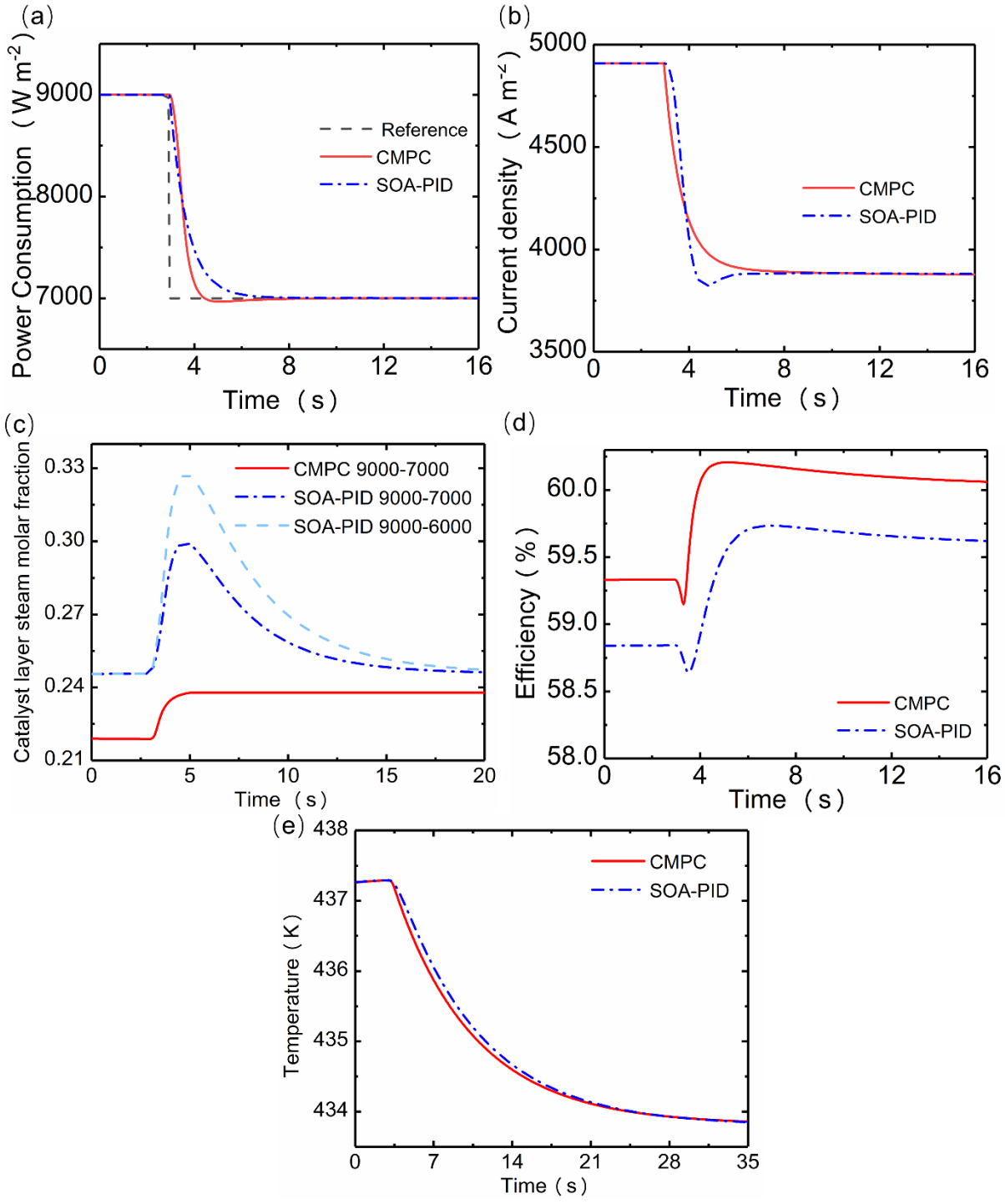

Fig. 9. (a) Power consumption transient response ; (b) Current density transient response; (c) Steam molar fraction transient response; (d) Energy efficiency transient response; (e) Operating temperature transient response.

Conclusion

In this study, the hydrogen recirculation system of HT-PEMEC is developed to avoid the introduction of additional steam at the cathode, which significantly reduces the thermal energy demand and improves energy efficiency. Moreover, the hierarchical model is utilized to study the transient behavior of the hydrogen recirculation system, which uses a multiphysics model to describe the electrolyzer cell as well as the sub-systems described by lumped parameter models. The application of the hierarchical model offers accurate transient behavior and avoids excessive computational costs. Additionally, compared to SOA-PID, the proposed cooperative model predictive control can not only provide higher efficiency but also prevent the reactant starvation problem. This study provides useful information to understand the dynamic behavior and control strategy design of HT-PEMEC.

The cooperative model predictive control strategy not only uses an artificial neural network to calculate the anode inlet gas flow rate corresponding to the maximum efficiency of the reference power consumption, but also constrains the maximum change rate of current density to avoid reactant starvation problems. However, the performance of the cooperative model predictive controller is dependent on the accuracy of the model estimation and the relationship between the input and output of the multiphysics model is not conveniently available, hence system identification is used to predict the dynamic behavior of the HT-PEMEC. Compared with the SOA-PID control strategy, the cooperative model predictive control strategy offers better dynamic performance and avoids the starvation problem of reactants as well as improves energy efficiency in dynamic processes. During the step response from 9000 W m^{-2} to 7000 W m^{-2}, the cooperative model predictive control strategy is approximately 1.2% more efficient compared to the SOA-PID control strategy.

The cooperative model predictive control strategy can be applied to other electrolyzer cell systems to optimize dynamic processes. Furthermore, the response and optimization of thermal

stresses should also be considered in subsequent research work.

Acknowledgments

M. NI thanks the grants (Project Number: PolyU 152064/18E and N_PolyU552/20) from Research Grant Council, University Grants Committee, Hong Kong SAR. Xi Li thanks the National Natural Science Foundation of China (grant numbers: U2066202, 61873323), the Science, Technology and Innovation Commission of Shenzhen Municipality (grant number: JCYJ20210324115606017), and the National Science Centre of the Republic of Poland for SONATA project (grant number: 2018/31/D/ ST8/00123).

References

[1] Marocco P, Ferrero D, Lanzini A, et al. The role of hydrogen in the optimal design of off-grid hybrid renewable energy systems[J]. Journal of Energy Storage, 2022, 46: 103893.

[2] Naik K R, Rajpathak B, Mitra A, et al. Power management scheme of DC micro-grid integrated with photovoltaic-Battery-Micro hydro power plant[J]. Journal of Power Sources, 2022, 525: 230988.

[3] Feng L, Zhang X, Li X, et al. Performance analysis of hybrid energy storage integrated with distributed renewable energy[J]. Energy Reports, 2022, 8: 1829-1838.

[4] He Y, Guo S, Zhou J, et al. Multi-objective planning-operation co-optimization of renewable energy system with hybrid energy storages[J]. Renewable Energy, 2022, 184: 776-790.

[5] He Y, Guo S, Zhou J, et al. Multi-objective planning-operation co-optimization of renewable energy system with hybrid energy storages[J]. Renewable Energy, 2022, 184: 776-790.

[6] Kumar S, Sharma R, Murthy S S, et al. Thermal analysis and optimization of stand-alone microgrids with metal hydride based hydrogen storage[J]. Sustainable Energy Technologies and Assessments, 2022, 52: 102043.

[7] Cao Y, Dhahad H A, ABo-Khalil A G, et al. Hydrogen production using solar energy and injection into a

solid oxide fuel cell for CO2 emission reduction; Thermoeconomic assessment and tri-objective optimization[J]. Sustainable Energy Technologies and Assessments, 2022, 50: 101767.

[8] Ibáñez-Rioja A, Puranen P, Järvinen L, et al. Simulation methodology for an off-grid solar–battery–water electrolyzer plant: Simultaneous optimization of component capacities and system control[J]. Applied Energy, 2021: 118157.

[9] Ni M, Leung M K H, Leung D Y C. Energy and exergy analysis of hydrogen production by a proton exchange membrane (PEM) electrolyzer plant[J]. Energy conversion and management, 2008, 49(10): 2748-2756.

[10] Hernández-Gómez Á, Ramirez V, Guilbert D, et al. Cell voltage static-dynamic modeling of a PEM electrolyzer based on adaptive parameters: Development and experimental validation[J]. Renewable Energy, 2021, 163: 1508-1522.

[11] Mohammadi A, Mehrpooya M. A comprehensive review on coupling different types of electrolyzer to renewable energy sources[J]. Energy, 2018, 158: 632-655.

[12] Karimi M B, Hooshyari K, Salarizadeh P, et al. A comprehensive review on the proton conductivity of proton exchange membranes (PEMs) under anhydrous conditions: Proton conductivity upper bound[J]. International Journal of Hydrogen Energy, 2021, 46(69): 34413-34437.

[13] Li H, Inada A, Fujigaya T, et al. Effects of operating conditions on performance of high-temperature polymer electrolyte water electrolyzer[J]. Journal of Power Sources, 2016, 318: 192-199.

[14] Toghyani S, Afshari E, Baniasadi E, et al. Thermal and electrochemical performance assessment of a high temperature PEM electrolyzer[J]. Energy, 2018, 152: 237-246.

[15] Jin Y, Wang T, Che X, et al. Poly (arylene pyridine) s: New alternative materials for high temperature polymer electrolyte fuel cells[J]. Journal of Power Sources, 2022, 526: 231131.

[16] Hansen M K, Aili D, Christensen E, et al. PEM steam electrolysis at 130 C using a phosphoric acid doped short side chain PFSA membrane[J]. International journal of hydrogen energy, 2012, 37(15): 10992-11000.

[17] Dong C, Xu X, Zhang J, et al. Proton transport of porous triazole-grafted polysulfone membranes for high temperature polymer electrolyte membrane fuel cell[J]. International Journal of Hydrogen Energy, 2022.

[18] Garbe S, Futter J, Schmidt T J, et al. Insight into elevated temperature and thin membrane application

for high efficiency in polymer electrolyte water electrolysis[J]. Electrochimica Acta, 2021, 377: 138046.

[19] Günay M E, Tapan N A, Akkoç G. Analysis and modeling of high-performance polymer electrolyte membrane electrolyzers by machine learning[J]. International Journal of Hydrogen Energy, 2022, 47(4): 2134-2151.

[20] Ruiz D D H, Sasmito A P, Shamim T. Numerical investigation of the high temperature PEM electrolyzer: effect of flow channel configurations[J]. ECS Transactions, 2013, 58(2): 99.

[21] Zhang Z, Xing X. Simulation and experiment of heat and mass transfer in a proton exchange membrane electrolysis cell[J]. International Journal of Hydrogen Energy, 2020, 45(39): 20184-20193.

[22] Bonanno M, Müller K, Bensmann B, et al. Evaluation of the Efficiency of an Elevated Temperature Proton Exchange Membrane Water Electrolysis System[J]. Journal of The Electrochemical Society, 2021, 168(9): 094504.

[23] Toghyani S, Baniasadi E, Afshari E. Numerical simulation and exergoeconomic analysis of a high temperature polymer exchange membrane electrolyzer[J]. International Journal of Hydrogen Energy, 2019, 44(60): 31731-31744.

[24] Nafchi F M, Baniasadi E, Afshari E, et al. Performance assessment of a solar hydrogen and electricity production plant using high temperature PEM electrolyzer and energy storage[J]. international journal of hydrogen energy, 2018, 43(11): 5820-5831.

[25] Ito H, Miyazaki N, Ishida M, et al. Efficiency of unitized reversible fuel cell systems[J]. International Journal of Hydrogen Energy, 2016, 41(13): 5803-5815.

[26] Xia L, Zhang C, Hu M, et al. Investigation of parameter effects on the performance of high-temperature PEM fuel cell[J]. International Journal of Hydrogen Energy, 2018, 43(52): 23441-23449.

[27] Xia L, Xu Q, He Q, et al. Numerical study of high temperature proton exchange membrane fuel cell (HT-PEMFC) with a focus on rib design[J]. International Journal of Hydrogen Energy, 2021, 46(40): 21098-21111.

[28] Brezak D, Kovač A, Firak M. MATLAB/Simulink simulation of low-pressure PEM electrolyzer stack[J]. International Journal of Hydrogen Energy, 2022.

[29] Falcão D S, Pinto A. A review on PEM electrolyzer modelling: Guidelines for beginners[J]. Journal of Cleaner Production, 2020, 261: 121184.

[30] Han B, Mo J, Kang Z, et al. Effects of membrane electrode assembly properties on two-phase transport and performance in proton exchange membrane electrolyzer cells[J]. Electrochimica Acta, 2016, 188: 317-326.

[31] Nie J, Chen Y, Boehm R F. Numerical modeling of two-phase flow in a bipolar plate of a PEM electrolyzer cell[C]//ASME International Mechanical Engineering Congress and Exposition. 2008, 48715: 783-788.

[32] Xu H, Chen B, Irvine J, et al. Modeling of CH4-assisted SOEC for H2O/CO2 co-electrolysis[J]. International Journal of Hydrogen Energy, 2016, 41(47): 21839-21849.

[33] Xu H, Chen B, Ni M. Modeling of direct carbon-assisted solid oxide electrolysis cell (SOEC) for syngas production at two different electrodes[J]. Journal of The Electrochemical Society, 2016, 163(11): F3029.

[34] Xia L, Zhang C, Hu M, et al. Investigation of parameter effects on the performance of high-temperature PEM fuel cell[J]. International Journal of Hydrogen Energy, 2018, 43(52): 23441-23449.

[35] Zhao D, He Q, Yu J, et al. Dynamic behaviour and control strategy of high temperature proton exchange membrane electrolyzer cells (HT-PEMECs) for hydrogen production[J]. International Journal of Hydrogen Energy, 2020, 45(51): 26613-26622.

[36] Zhao D, He Q, Wu X, et al. Modeling and optimization of high temperature proton exchange membrane electrolyzer cells [J]. Int J Green Energy 2021:1-12.

[37] Zhang L, Li X, Jiang J, et al. Dynamic modeling and analysis of a 5-kW solid oxide fuel cell system from the perspectives of cooperative control of thermal safety and high efficiency[J]. international journal of hydrogen energy, 2015, 40(1): 456-476.

[38] Zhang L, Jiang J, Cheng H, et al. Control strategy for power management, efficiency-optimization and operating-safety of a 5-kW solid oxide fuel cell system[J]. Electrochimica Acta, 2015, 177: 237-249.

[39] Li J, Zoghi M, Zhao L. Thermo-economic assessment and optimization of a geothermal-driven tri-generation system for power, cooling, and hydrogen production[J]. Energy, 2022: 123151.

[40] Wang Z, Wang X, Chen Z, et al. Energy and exergy analysis of a proton exchange membrane water electrolysis system without additional internal cooling[J]. Renewable Energy, 2021, 180: 1333-1343.

[41] Ni M, Leung M K H, Leung D Y C. Energy and exergy analysis of hydrogen production by solid oxide steam electrolyzer plant[J]. International Journal of Hydrogen Energy, 2007, 32(18): 4648-4660.

[42] Arbabi F, Montazeri H, Abouatallah R, et al. Three-dimensional computational fluid dynamics modelling of oxygen bubble transport in polymer electrolyte membrane electrolyzer porous transport layers[J]. Journal of The Electrochemical Society, 2016, 163(11): F3062.

[43] Toghyani S, Afshari E, Baniasadi E. Three-dimensional computational fluid dynamics modeling of proton exchange membrane electrolyzer with new flow field pattern[J]. Journal of Thermal Analysis and Calorimetry, 2019, 135(3): 1911-1919.

[44] Torreglosa J P, Jurado F, García P, et al. PEM fuel cell modeling using system identification methods for urban transportation applications[J]. International journal of hydrogen energy, 2011, 36(13): 7628-7640.

[45] Zhao D, He Q, Yu J, et al. A data-driven digital-twin model and control of high temperature proton exchange membrane electrolyzer cells[J]. International Journal of Hydrogen Energy, 2022.

[46] Mayne D Q. Model predictive control: Recent developments and future promise[J]. Automatica, 2014, 50(12): 2967-2986.

[47] Mayne D Q, Rawlings J B, Rao C V, et al. Constrained model predictive control: Stability and optimality[J]. Automatica, 2000, 36(6): 789-814.

[48] Chen C, Li J, Luo J, et al. Seeker optimization algorithm for optimal control of manipulator[J]. Industrial Robot: An International Journal, 2016, 43(6): 677-686.

[49] Parvaneh H, Dizgah S M, Sedighizadeh M, et al. Load frequency control of a multi-area power system by optimum designing of frequency-based PID controller using seeker optimization algorithm[C]//2016 6th Conference on Thermal Power Plants (CTPP). IEEE, 2016: 52-57.

[50] Carmo M, Fritz D L, Mergel J, et al. A comprehensive review on PEM water electrolysis[J]. International journal of hydrogen energy, 2013, 38(12): 4901-4934.

[51] Elwan H A, Thimmappa R, Mamlouk M, et al. Applications of poly ionic liquids in proton exchange membrane fuel cells: A review[J]. Journal of Power Sources, 2021, 510: 230371.

[52] Qin S J, Badgwell T A. A survey of industrial model predictive control technology[J]. Control engineering practice, 2003, 11(7): 733-764.

[53] Zhu Y, Dai C, Chen W. Seeker optimization algorithm for several practical applications[J]. International Journal of Computational Intelligence Systems, 2014, 7(2): 353-359.